Analytical Methods

# A near-infrared carbon dioxide sensor system using a compact folded optical structure for deep-sea natural gas hydrates exploration



| | |
|---|---|
| Journal: | *Analytical Methods* |
| Manuscript ID | AY-ART-08-2018-001776.R1 |
| Article Type: | Paper |
| Date Submitted by the Author: | 05-Sep-2018 |
| Complete List of Authors: | Liu, Zhiwei; Jilin University, College of Electronic Science and Engineering<br>Zheng, Chuan-Tao; Jilin University, College of Electronic Science and Engineering<br>Chen, Chen; Jilin University, College of Instrumentation & Electrical Engineering<br>Xie, Hongtao; Jilin University, College of Electronic Science and Engineering<br>Ren, Qiang; Jilin University, College of Instrumentation & Electrical Engineering<br>Ye, Weilin; Shantou University<br>Wang, Yi-Ding; Jilin University, College of Electronic Science and Engineering<br>Tittel, Frank; Rice University, Electrical and Computer engineering |
| | |

Analytical Methods

ARTICLE

# A near-infrared carbon dioxide sensor system using a compact folded optical structure for deep-sea natural gas hydrates exploration

Received 00th January 20xx,
Accepted 00th January 20xx

DOI: 10.1039/x0xx00000x

www.rsc.org/

Zhiwei Liu,[ad] Chuantao Zheng,[*ad] Chen Chen,[b] Hongtao Xie,[ad] Qiang Ren,[b] Weilin Ye,[c] Yiding Wang [ad] and Frank K. Tittel [e]

The detection of dissolved gas (e.g. carbon dioxide ($CO_2$), methane ($CH_4$)) in seawater is important for deep-sea natural gas hydrates exploration, which requires that the sensor especially the optical structure should be of compact size and capable of operation under deep-sea environment. A compact optical structure with simple beam alignment and tracing method was proposed for tunable laser absorption spectroscopy (TLAS) based gas measurements, in order to minimize sensor size and ease beam alignment/tracing procedure for deep-sea operation. A near-infrared $CO_2$ sensor system was developed based on the compact optical structure. A distributed feedback (DFB) laser centered at 6361.3 $cm^{-1}$ and a multi-pass gas cell (MPGC) with an effective optical path length of 29.8 m were employed. The sensor system was integrated as standalone equipment by customizing an aluminum baseplate for a stable field operation. A series of experiments were carried out to assess the performance of the sensor system. A limit of detection (LoD) of ~ 7.1 parts-per-million in volume (ppmv) at a 0.4 s averaging time was obtained, and the LoD was reduced to ~ 277 parts-per-billion in volume (ppbv) at an optimum averaging time of 153.6 s. Considering gas mixing time, the rise and fall time were measured to be ~ 290 s and ~200 s, respectively. The proposed compact sensor structure provides the basis for the further development of a sensor system for dissolved $CO_2$ detection with a LoD of ppbv via the use of a mid-infrared tunable laser.

## 1. Introduction

Natural gas hydrates, regarded as a new type of energy material with great potential application in the 21th century, have been begun to be explored on the worldwide seafloor.[1,2] Before widely mining and utilization of this sort of clean and precious resource, high resolution detection and analysis of natural gas hydrates are also meaningful. Under a specific condition, gas hydrates on the seabed can decompose and generate several gas species, such as methane ($CH_4$), carbon dioxide ($CO_2$) and hydrogen sulphide ($H_2S$). Therefore, quantitative analysis of gas species dissolved in seawater near the seabed is in great demand for the exploration of natural gas hydrates. In recent years, two methods, including marine deep-tow seismic technique[3] and spectroscopy-based geochemical detection[4] were employed to measure gas species escaping from the seabed for the content analysis of natural gas hydrates. However, these reported techniques cannot achieve both high accuracy and *in situ* measurements as required. In addition, these techniques usually need large-size and complicated facilities, increasing the difficulty in gas detection under water. An infrared laser absorption spectroscopy (LAS) based gas detection approach[5] is widely used in atmospheric and environmental monitoring, which has a high accuracy up to the level of parts per billion in volume (ppbv) and a non-contact *in situ* detection performance. Therefore a compact LAS sensor system aiming at deep-sea resource exploration is required for the detection of the gas species extracted by an underwater gas-liquid separator.

Tunable laser absorption spectroscopy (TLAS) in the infrared[6-8] was widely used for trace gas detection and has been applied in sensitive gas measurements in a variety of fields, such as, environmental monitoring[9-11] and industrial application.[12,13] A TLAS based gas sensor system[14,15] consists of a light source targeting an absorption line of a specific gas, a gas cell for the interaction between gas molecule and infrared light, and a detector for the transformation from a lightwave to an electrical signal. Optimum structure related to these three components for beam alignment and tracing is important for improving sensor performance. Furthermore sensor size and design complexity are other factors that should be considered in establishing the optical path. A near-infrared source produces a laser beam via a pigtail fiber, which can be

[a] State Key Laboratory of Integrated Optoelectronics, College of Electronic Science and Engineering, Jilin University, 2699 Qianjin Street, Changchun, 130012, P.R. China.
[b] College of Instrumentation & Electrical Engineering, Jilin University, 938 Ximinzhu Street, Changchun, 130021, P.R. China.
[c] College of Engineering, Shantou University, 243 Daxue Road, Shantou 515063, China.
[d] Jilin Provincial Engineering Research Center of Infrared Gas Sensing Technique, 2699 Qianjin Street, Changchun 130012, China.
[e] Department of Electrical and Computer Engineering, Rice University, 6100 Main Street, Houston, TX 77005, USA.
*Corresponding author. E-mail: zhengchuantao@jlu.edu.cn (C. Zheng)

connected directly to a cell through a fiber connector. However, for a mid-infrared laser, optical components and a proper alignment method are required. Generally, the reported optical structure[16-18] used a dichroic mirror to combine the invisible infrared light with a visible laser beam for easy alignment. Nevertheless, the dichroic mirror results in an attenuation of the laser power so that weakens the optical transfer efficiency of the system. In addition, because of the light scattering caused by the dichroic mirror, some extra lenses may be needed to focus the laser beam which brings more complexity to the optical structure.

In order to minimize sensor size and facilitate the beam alignment procedure (required for some special application, e.g. deep-sea gas measurement), a more simple and compact optical structure for TLAS-based *in situ* gas detection was proposed and functionally verified. In comparison with the reported structure in [16], the dichroic mirror and the focusing lens were removed in order to reduce the sensor size and a new near-infrared $CO_2$ sensor system was developed. A distributed feedback (DFB) laser centred at 6361.3 $cm^{-1}$ and a multi-pass gas cell (MPGC)[19] with an effective optical path length of 29.8 m were employed. Moreover, the sensor system was integrated as a standalone equipment by adopting a custom aluminium baseplate for a convenient deployment and stable operation of the sensor. A series of experiments were carried out to assess the performance of the sensor system, which provides the basis for the further development of a mid-infrared $CO_2$ sensor system with a limit of detection (LoD) of ppbv via the use of a mid-infrared tuneable laser.

## 2. $CO_2$ sensor system configuration for deep-sea operation

### 2.1. Deep-sea sensor design requirement

Different from the TLAS-based sensors operating on land, several problems need to be solved when the technique is going to be used in the deep-sea environment. Firstly, all components of the sensor system should be integrated into a standalone equipment as small as possible so that it can be transported and hauled under seawater conveniently. Afterwards, in order to carry out *in-situ* detection, the gas dissolved in seawater should be extracted out and then injected immediately into the MPGC for detection. Moreover, in allusion to the ultrahigh hydraulic pressure and relatively low temperature at thousands of meters under seawater, a towed body should be specially designed to carry the sensor system.

Considering the problems mentioned above and employing the marine deep-tow technique, a schematic for deep-sea TLAS-based gas detection using a gas-liquid separator is preliminarily described in Fig. 1. A pressure-proof shell acts as the towed body to carry a gas-liquid separator, a TLAS-based sensor system and a waste gas treatment system. The gas-liquid separator extracts the dissolved gas from seawater and then injects it into the sensor. After reaction with infrared

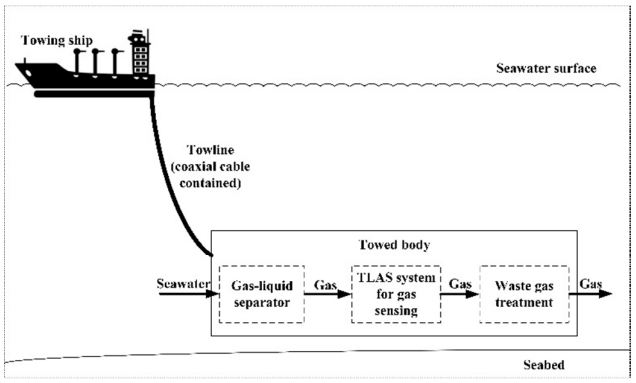


Fig. 1 Schematic of the deep-sea gas detection employing the deep-tow technique and a gas-liquid separator.

light, the gas output from the sensor flows to the waste gas treatment system. A coaxial-cable connecting the towed body and a towing ship boat not only performs as a towline, but also transmit sensing signal from the sensor to the upper control computer on the deck. In order to minimize the effect of surrounding temperature change undersea on the sensor performance, the temperature of the gas cell is heated to be 2-3 $^{o}C$ above the surrounding temperature, and the detection results are temperature-compensated through software. With the above design concept, a deep-sea in situ gas sensor based on TLAS technique is realized in this paper, and the focus of our design is to propose a compact folded optical structure, minimize the dimension size and validate the normal operation.

### 2.2. Compact folded optical structure for beam alignment and tracing

In order to enhance the mechanical stability, an aluminium plate was used to mount the optical sub-system, which consists of a light source, a gas cell, a photoelectric detector and three reflectors. The MPGC, with a special dense spot pattern, provides a sealed environment for the interaction between gas molecules and the infrared light. The cell offers a 29.8 m effective optical path length after 215 reflections with a physical size of 20×16×5 $cm^3$. A near-infrared DFB laser was used as the optical source and two three-dimensionally adjustable mirrors (M1 and M2) were employed to guide the infrared beam into the MPGC. The output beam was focused onto an In-Ga-As (IGA) detector (Thorlabs, model PDA10D-EC) using a parabolic mirror (PM, diameter 25.4 mm, focal length 50.8 mm).

A 635 nm visible laser was used for beam alignment and on account of the absence of dichroic mirror, a novel beam-tracing method was employed. Fig. 2 shows the optical alignment structure and the red and grey lines represent the infrared and visible beam, respectively. The MPGC, which is regarded to be the key unit of the optical sub-system, was fixed on an aluminium baseplate. As described in Fig. 2(a), the visible light from the alignment laser entered the MPGC according to a specific position and angle to obtain a mode

 

pattern shown in the inset by carefully adjusting M2 and the output beam was focused on the IGA by the PM. Once a

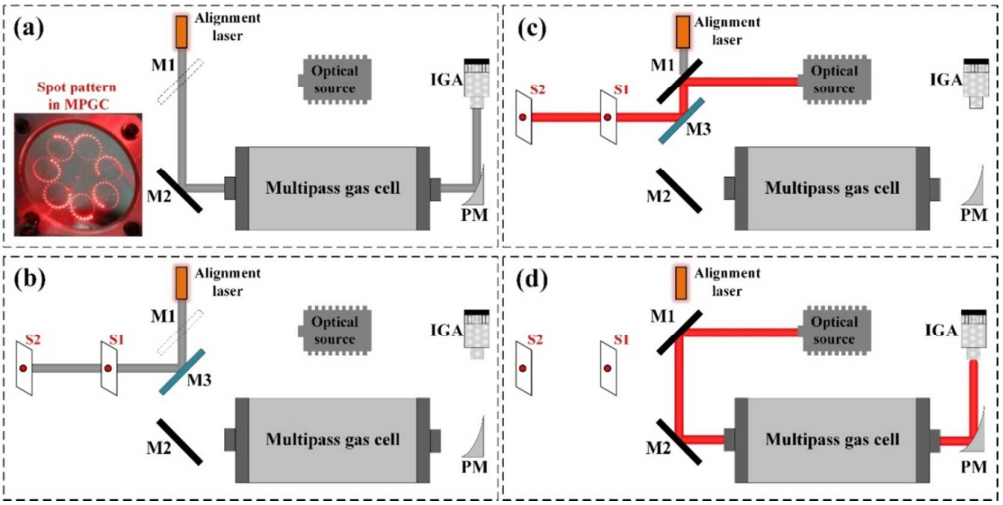


Fig. 2 Optical path alignment process. (a) Optical path alignment using the visible light beam. (b) Representation of the alignment beam path by marking spots on paperboards. (c) Alignment of the infrared beam according to the marked spots on paperboards. (d) The aligned optical path structure.

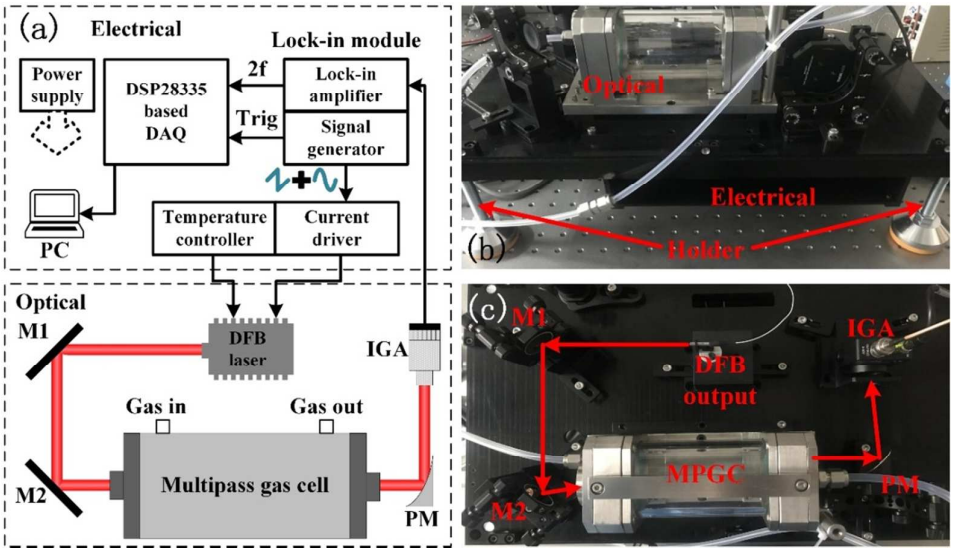


Fig. 3 (a) Schematic of the $CO_2$ sensor system including an electrical and an optical sub-system. DFB: distributed feedback; IGA: InGaAs detector; M: plane mirror; PM: parabolic mirror. (b) Photograph of the integrated sensor system. (c) Top view of the optical structure.

correct light path was achieved based on the visible beam, the next step is to align the infrared beam with the visible beam. For this purpose, the mirror M1 was installed on a 90° flip mount (Thorlabs, model FM90/M), which can repetitively switch the incident beam between the alignment laser and the DFB laser. A plane mirror (M3) was placed between M1 and M2 to reflect the incident beam to the direction opposite to the optical sub-system for alignment observation. Along the reflected optical path by M3, two stably-fixed paperboards were used to mark the spot positions (S1, S2) by painting two dots. This can be considered as a description of the light path of the visible beam as depicted in Fig. 2(b). As shown in Fig. 2(c), the DFB laser was powered on and a thermo-sensitive laser viewing card was used to observe the spot of the infrared light. In this procedure, the position and reflection angle of M1 were carefully adjusted to make sure that the infrared spots on M1, M3, S1 and S2 coincide with the visible spots, respectively. By adjusting M1, the spot positions of these two beams can be observed with high accuracy. A simultaneous monitor on the IGA output and a slight adjustment of M1 are also needed to obtain a final optical path as shown in Fig. 2(d).

### 2.3. Sensor design

A wavelength modulation spectroscopy (WMS)[20-22] based $CO_2$ sensor system was developed based on the compact folded optical structure. As depicted in Fig. 3(a), the system consists of an electrical and an optical sub-system. In the electrical part, a laser drive module (Wavelength Electronics, model LDTC0520) including a temperature controller and a current driver were employed for stabilizing the laser temperature and supplying a laser current. A dual-channel lock-in module was used to generate a saw-tooth scan signal superimposed by a sinusoid modulation signal for the current driver and also to extract the 2*f* signal from the IGA output signal. Another saw-tooth signal synchronized with the scan signal generated by the lock-in module was converted to a square-wave signal in order to trigger data sampling. A digital signal processor (DSP, Texas Instruments, model TMS320F28335) based data acquisition module was used for 2*f* signal acquisition. The DSP also delivered the 2*f* signal, 2*f*-amplitude and concentration to a laptop for data-record and post analysis. Furthermore, a compact power supply module with a direct current supply voltage of 24 V was developed for the whole sensor system with a total power consumption of ~ 36W. Fig. 3(b) shows the assembled equipment with a physical size of 52×30×27 $cm^3$ including the optical sub-system on the baseplate and the electrical sub-system. Fig. 3(c) is the top view of the optical path structure described in Sect. 2.1.

### 2.4. Laser characterization and optimization

Two main considerations were made for the choice of the 6359.96 $cm^{-1}$ absorption line for $CO_2$ concentration measurements.[23,24] Firstly, a near-infrared laser with mature fabrication technique and low cost is preferred to verify the effectiveness of the proposed optical structure. Also, simulations of the absorbance of $CO_2$ and water vapour were both performed at a typical laboratory condition based on the HITRAN database. The 6359.96 $cm^{-1}$ line with a strength of $1.977\times10^{-23}$ cm/molecule is the strongest line and exhibits no overlap with water vapour absorption nearby.

The integrated current driver and temperature controller operated at an external voltage driving and internal temperature control mode and received a scan and modulation signal from the lock-in module. An additional circuit was used to change the ratio between the input voltage and output current to be 18.5 mA/V from the default value of 250 mA/V for a high current accuracy. As shown by the spectrum results depicted in Fig. 4(a), the laser operated at 28℃ can be tuned to emit a wavenumber range from 6359.5 $cm^{-1}$ to 6360.2 $cm^{-1}$, covering the $CO_2$ absorption line at 6359.96 $cm^{-1}$ (@58.3 mA). At a temperature of 28℃, the emission spectrum of the laser within a driving current range of 45 − 80 mA is shown in Fig. 4(b). A scan current with a range of 45 − 75 mA and a frequency of 10 Hz was used to drive the DFB laser.

To obtain the optimum sensing performance, a suitable modulation depth should be determined, which corresponds to the maximum 2*f* signal amplitude. A gas mixing system (Environics, series 4000) was used to generate a $CO_2$ sample of 4000 ppmv by diluting a standard 1% $CO_2$ with pure nitrogen ($N_2$). The experiment was conducted at a pressure of 1 atm. By applying a sinusoidal modulation signal of 5 kHz with different modulation amplitudes and the obtained 2*f* signal and its amplitude were recorded. The maximum 2*f* signal amplitude was achieved when the modulation

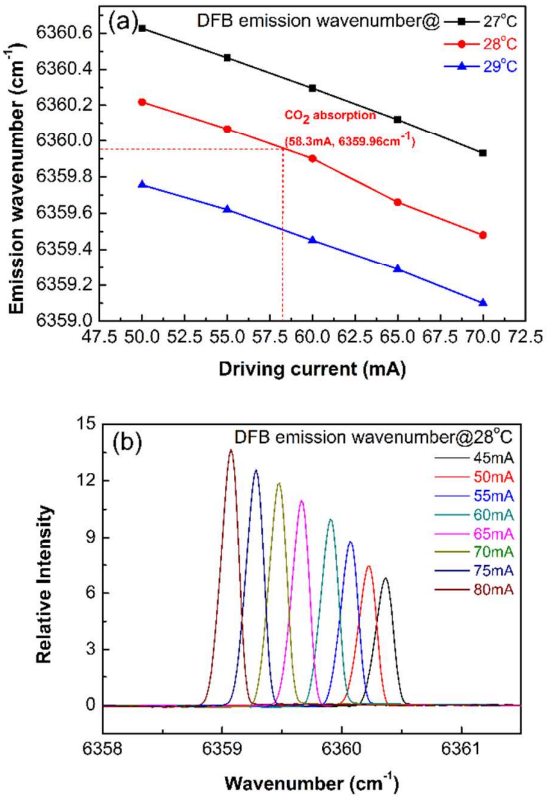


Fig. 4 Characterization of the DFB laser. (a) Laser emission wavenumber at different current and temperature. (b) Laser emission spectrum profile at different drive current at 28℃.

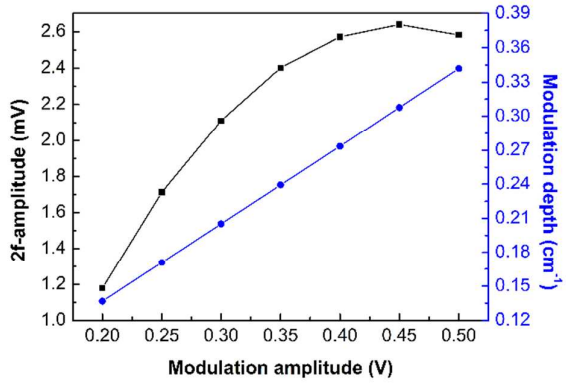


Fig. 5 The 2*f* signal amplitude and modulation depth as a function of the modulation amplitude for a 4000 ppmv $CO_2$ sample.

depth was 0.31 $cm^{-1}$, corresponding to a modulation amplitude of 0.45 V, as depicted in Fig. 5.

## 3. Experiment and results

### 3.1. Sensor calibration

A saw-tooth signal with a voltage range of 2 − 3.8 V and a frequency of 10 Hz superimposed by a 5 kHz sinusoidal

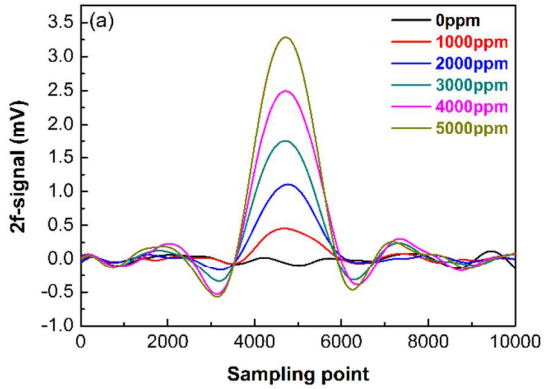


Stability

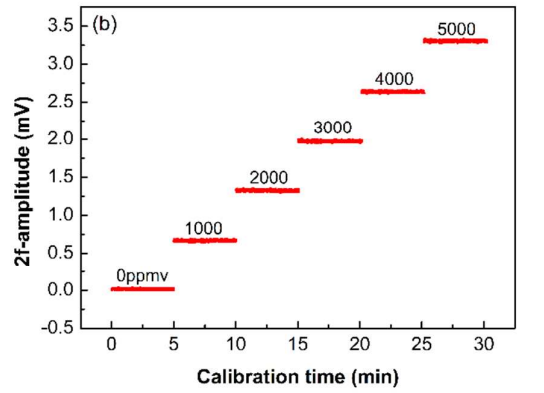


Fig. 6 (a) Measured 2*f* waveforms at different $CO_2$ concentration levels. (b) Measured curves of the 2*f*-amplitudes versus calibration time for the 0, 1000, 2000, 3000, 4000, 5000 ppmv $CO_2$ samples.

modulation signal with an amplitude of 0.45 V was applied on the DFB laser. A gas mixing system was used to generate six $CO_2$ samples with a concentration range of 0 – 5000 ppmv. At each concentration level, the 2*f* waveform and the measured 2*f* signal amplitude were recorded for 5 minutes' intervals, as shown in Fig. 6. Then, the 2*f*-amplitude of each concentration were averaged and plotted as a function of the theoretical concentration value. As depicted in Fig. 7, by a linear data-fitting, an equation between the 2*f*-amplitude (i.e. max(2*f*)) and the gas concentration (*C*) was obtained

$$C = 1520.41196\max(2f) - 14.03115 \quad (1)$$

Using the measured 2*f*-amplitude, the $CO_2$ concentration can be determined based on Eq. (1).

When a $CO_2$ sample with a specific concentration is generated by mixing the standard $CO_2$ with $N_2$, the gas mixing system may bring concentration fluctuation to the gas prepared. Therefore the stability of the sensor system was tested by injecting $N_2$ into the MPGC to eliminate the influence of the fluctuation of the gas concentration. An experiment lasting ~ 30 min was performed and the measured concentration with a data sampling period of 0.4 s was recorded. An Allan deviation analysis was employed to characterize the stability and the limit of detection (LoD). Fig. 8 exhibits the time series of the measured concentration levels

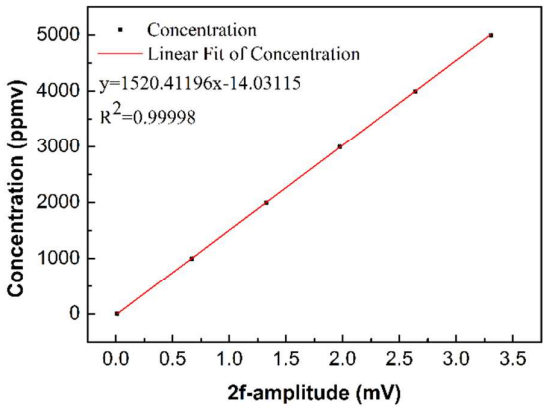


Fig. 7 Measured data dots and fitting curve of the $CO_2$ concentration versus 2*f*-amplitude.

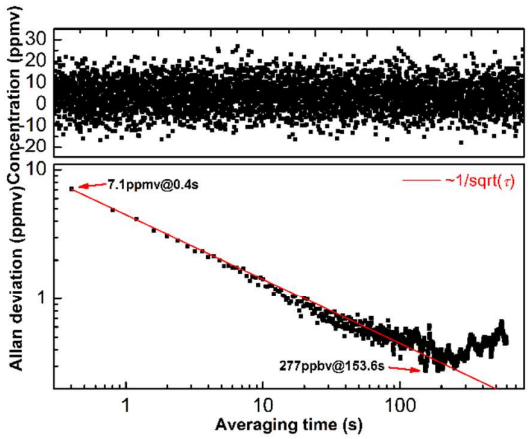


Fig. 8 Measured concentration of a 0 ppmv $CO_2$ sample and the Allan deviation analysis of the sensor system.

and the Allan deviation versus the averaging time $\tau$. A LoD of ~ 7.1 ppmv for a 0.4 s averaging time was achieved and an optimum averaging time of 153.6 s corresponding to a LoD of ~ 277 ppbv was observed. The red line proportional to 1/sqrt($\tau$) expresses the theoretical performance of a system impacted by White-Gaussian noise only.

A simulation of the $CO_2$ absorbance based on the HITRAN database was performed for a LoD concentration level of 7.1 ppmv. The other crucial parameters, including temperature, pressure and optical path length, were all set to be the same with that employed in the experiment. The concentration level of 7.1 ppmv leads to a $CO_2$ absorbance of $4\times10^{-5}$, which demonstrates that the sensor has a relatively good performance after parameter optimization.

### 3.2. Response time

A continuous dynamic measurement was performed for ~ 25 min to determine the response behavior of the sensor system. The gas mixing system was used to produce three $CO_2$ samples whose concentration levels were 1300, 4000, 2200 ppmv,

respectively. Fig. 9 shows the measured concentration results when the concentration level was increased from 1300 to 4000

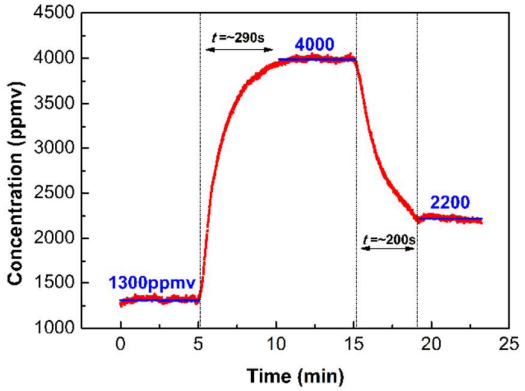


Fig. 9 Response time measurements by switching gas samples with different concentration levels using the gas mixing system.

ppmv and then was decreased to 2200 ppmv. Every gas sample was measured for ~ 5 min after the sensor reading was stable. During the test, the total flow rate of the sensor system was 130 mL/min. The MPGC has a volume of ~ 340 mL and was connected with the outlet of the gas mixing system by a pipe line with a volume of ~ 80 mL. Hence, the gas flow time was ~ 3 min. In addition, the gas preparation time of the mixing system to obtain a stable concentration should also be considered. According to the experimental results in Fig. 9, the rise time was measured to be ~ 290 and fall time was ~ 200 s without excluding the gas mixing time.

### 3.3. Deployment of the sensor system

Another four gas cylinders with a standard CO2 concentration level of 1500, 2500, 3500, 4500 ppmv were used to verify the detection performance and the linearity of the sensor system. Each gas sample was measured for ~ 5 min. For each group of measurement data, the averaged value was plotted versus the actual concentration of the sample with error bar as depicted in Fig. 10(a). The red line in the Fig. 10(a) represented by $y = x$ indicates that the detection results of these gas samples had a good linearity.

A detection of human breath gas analysis was performed to observe the sensor behaviour. An oil-free vacuum pump (KNF Neuberger Inc., Model N816.3KN.18) was employed to pump the human breath from the inlet of the MPGC. The response of the sensor system was recorded and exhibited in Fig. 10(b). Each peak represents a human breath. The two blue dash lines represent the maximum $CO_2$ concentration and the minimum concentration, respectively. The $CO_2$ concentration in the indoor atmosphere was ~ 400 ppmv according to the baseline of the data. The concentration of the breath $CO_2$ gas was ~ 5.9%. Also, by analysing the detailed data recorded during a concentration change, the rise and fall time were determined to be ~ 10 s excluding the gas mixing time.

## 4. Conclusions

Aiming at deep-sea natural gas hydrates exploration, we reported the development of a compact folded optical structure for beam tracing and alignment, which can be employed in both near and mid-infrared gas detection based on TLAS. The established optical path is suitable for a sensor system using an MPGC without

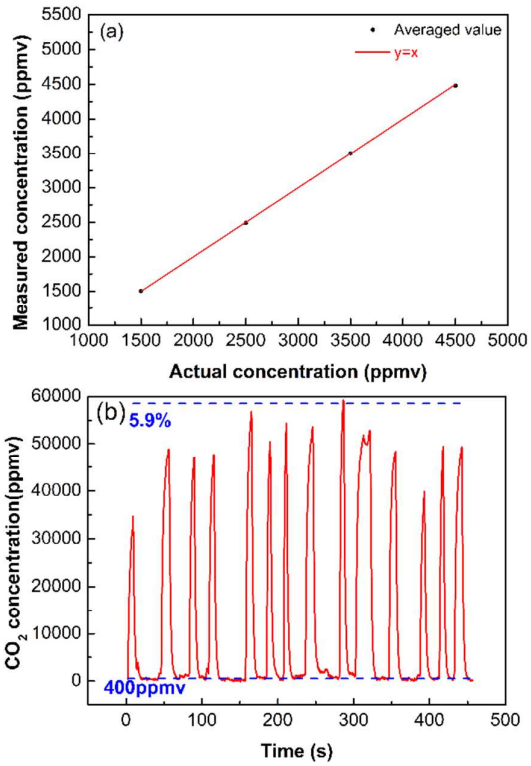


Fig. 10 Deployment of the $CO_2$ sensor system. (a) Measured $CO_2$ concentration of four gas samples versus the theoretical concentration of 1500, 2500, 3500, 4500 ppmv. (b) Measured $CO_2$ concentration by pumping human breath gas into the cell.

a fibre coupler for light injection. Based on this structure, a $CO_2$ sensor system consisting of a DFB laser, an IGA detector and a MPGC with a 29.8 m optical path length was developed. All the components of both the optical sub-system and the electrical sub-system were assembled into a standalone system for deployment. The DFB laser was operated to target a $CO_2$ absorption line located at 6359.96 $cm^{-1}$. Sensor calibration within a wide concentration range of 0 – 5000 ppmv was performed and a series of experiments were carried out to assess the performance of the system. Based on an Allan deviation analysis, a LoD of ~7.1 ppmv at a 0.4 s averaging time was obtained and at an optimum averaging time of 153.6 s, the LoD was reduced to ~ 277 ppbv. The rise and fall time at a dynamic operation were measured to be ~ 290 s and ~ 200 s, respectively, including the gas preparation time of the gas mixing system.

## Conflicts of interest

There are no conflicts to declare.

## Acknowledgements

The authors wish to express their gratitude to the National Key R&D Program of China (No. 2016YFC0303902), National Natural Science Foundation of China (Nos. 61775079, 61627823), Key Science and Technology R&D Program of Jilin Province, China (No. 20180201046GX), Science and Technology Planning Project of Guangdong Province, China (No. 2017A020216011), Industrial Innovation Program of Jilin Province, China (No. 2017C027), and National Science Foundation (NSF) ERC MIRTHE award and the Robert Welch Foundation (No. R4925U).

## References

1 B.U. Haq, Methane in the Deep Blue Sea, *Science,* 1999, **285**, 543-544.
2 M. Parlaktuna and T. Erdogmus, Natural Gas Hydrate Potential of the Black Sea, *Energy sources*, 2010, **23**, 203-211.
3 S. Ker, Y. Le Gonidec, B. Marsset, G.K. Westbrook, D. Gibert and T.A. Minshull, Fine-scale gas distribution in marine sediments assessed from deep-towed seismic data, *Geophys. J. Int.*, 2014, **196**, 1466-1470.
4 W.J. Lu, I.M. Chou and R.C. Burruss, Determination of methane concentrations in water in equilibrium with sI methane hydrate in the absence of a vapor phase by in situ Raman spectroscopy, *Geochim. Cosmochim. Ac.*, 2008, **72**, 412–422.
5 F. Song, C.T. Zheng, W.H. Yan, Y.W. Lin, Y.D. Wang and F.K. Tittle, Interband cascade laser based mid-infrared methane sensor system using a novel electrical-domain self-adaptive direct laser absorption spectroscopy (SA-DLAS), *Opt. express*, 2017, **25**, 31876-31888.
6 J.A. Silver, Frequency-modulation spectroscopy for trace species detection: theory and comparison among experimental methods, *Appl. Opt.*, 1992, **31**, 707–717.
7 P. Werle, A review of recent advances in semiconductor laser based gas monitors, *Spectrochim. Acta. A*, 1998, **54**, 197–236.
8 S. Schilt, L. Thévenaz and P. Robert, Wavelength modulation spectroscopy: combined frequency and intensity laser modulation, *Appl. Opt.*, 2003, **42**, 6728–6738.
9 G. Wysocki, Y. Bakhirkin, S. So, F.K. Tittel, C.J. Hill, R.Q. Yang and M.P. Fraser, Dual interband cascade laser based trace-gas sensor for environmental monitoring, *Appl. Opt.*, 2007, **46**, 8202–8210.
10 M.N. Fiddler, I. Begashaw, M.A. Mickens, M.S. Collingwood, Z. Assefa and S. Bililign, Laser spectroscopy for atmospheric and environmental sensing, *Sensors*, 2009, **9**, 10447–10512.
11 R.F. Curl, F. Capasso, C. Gmachl, A.A. Kosterev, B. McManus, R. Lewicki, M.Pusharsky, G. Wysocki and F.K. Tittel, Quantum cascade lasers in chemical physics, *Chem. Phys. Lett. Front. Artic.*, 2010, **487**, 1–18.
12 G. Wysocki, A.A. Kosterev and F.K. Tittel, Spectroscopic trace-gas sensor with rapidly scanned wavelengths of a pulsed quantum cascade laser for in situ NO monitoring of industrial exhaust systems, *Appl. Phys. B*, 2005, **80**, 617–625.
13 M. Lewander, Z.G. Guan, L. Persson, A. Olsson and S. Svanberg, Food monitoring based on diode laser gas spectroscopy, *Appl. Phys. B*, 2008, **93**, 619–625.
14 S. Tranchart, I.H. Bachir and J.L. Destombes, Sensitive trace gas detection with near-infrared laser diodes and an integrating sphere, *Appl. Opt*., 1996, **35**, 7070-4.
15 B. Li, Q.X. He, H.F. Liu and Y.D. Wang, A trace gas sensor using near infrared distributed feedback laser at 1654nm, *Laser physics*, 2015, **25**, 086001.
16 C.G. Li, C.T. Zheng, L. Dong, W.L. Ye, F.K. Tittel and Y.D. Wang, Ppb-level mid-infrared ethane detection based on three measurement schemes using a 3.34-μm continuous-wave interband cascade laser, *Appl. Phys. B*, 2016, **122**, 185.
17 C.G. Li, L. Dong, C.T. Zheng and F.K. Tittel, Compact TDLAS based optical sensor for ppb-level ethane detection by use of a 3.34μm room-temperature CW interband cascade laser, *Sens. Actuators B Chem.*, 2016, **232**, 188–194.
18 W.L. Ye, C.G. Li, C.T. Zheng, N.P. Sanchez, A.K. Gluszek, A.J. Hudzikowski, L. Dong, R.J. Griffin and F.K. Tittel, Mid-infrared dual-gas sensor for simultaneous detection of methane and ethane using a single continuous-wave interband cascade laser, *Opt. express*, 2016, **24**, 16973-16985.
19 K. Liu, L. Wang, T. Tan, G.S. Wang, W.J. Zhang, W.D. Chen and X.M. Gao, Highly sensitive detection of methane by near-infrared laser absorption spectroscopy using a compact dense-pattern multi-pass cell, *Sens. Actuators B Chem.*, 2015, **220**, 1000-1005.
20 O.B. Daniel, E.P. Mark and S.B. David, Frequency modulation multiplexing for simultaneous detection of multiple gases by use of wavelength modulation spectroscopy with diode lasers, *Appl. Opt.*, 1998, **37**, 2499-2501.
21 H.X. Cui, Z.H. Du, W.L. Chen, R.B. Qi and K.X. Xu, Applying diode laser wavelength modulation spectroscopy to detect oxygen concentration, *Laser. Eng.*, 2008, **18**, 263-270.
22 A. Carpf and G.N. Rao, Absorption and wavelength modulation spectroscopy of NO2 using a tunable, external cavity continuous wave quantum cascade laser, *Appl. Opt.*, 2009, **48**, 408-413.
23 T. Asakawa, N. Kanno and K. Tonokura, Diode Laser Detection of Greenhouse Gases in the Near-Infrared Region by Wavelength Modulation Spectroscopy: Pressure Dependence of the Detection Sensitivity, *Sensors*, 2010, **10**, 4686-4699.
24 W. Gong, X. Ma, G. Han, C.Z. Xiang, A.L. Liang and W.D. Fu, Method for wavelength stabilization of pulsed difference frequency laser at 1572 nm for $CO_2$ detection lidar, *Opt. express*, 2015, **23**, 6151-6170.

Near-infrared carbon dioxide sensor system using a compact folded optical structure for deep-sea natural gas hydrates exploration